

Model calculations of inverse photoemission

W. L. Schaich

*Department of Physics, Indiana University, Bloomington, Indiana 47405
and Materials Research Institute, Indiana University, Bloomington, Indiana 47405*

(Received 9 September 1991)

The electron-energy distribution of inverse-photoemission yield at fixed photon energy is calculated for a one-dimensional model of the potential energy that allows for both a bulk band gap and a surface barrier with an image-potential tail. By varying the width of the band gap in this model, surface states can be transformed into surface resonances. The variations of peak locations, strengths, and widths during such transformations are examined in detail and compared with the predictions of simpler models.

I. INTRODUCTION

In the past few years there has been much progress in understanding the variety of surface states that exist on different crystal faces of metals.^{1,2} A wealth of data from inverse photoemission and other spectroscopies has been collected and can be systematically assimilated with the help of a multiple-scattering picture that portrays an electron in a surface state as trapped between two totally reflecting barriers provided by a bulk band gap and by the surface potential (with a image-potential tail).³⁻⁶ The mathematical condition for constructive interference of the multiple reflections back and forth between these barriers defines the surface-state energy location. The inputs necessary for a quantitative evaluation of these locations are the (complex-valued) reflection amplitudes for scattering from each barrier, which may be modeled and calculated separately. Considerable success has been obtained using fairly simple models of the barriers.⁷⁻⁹

However, these efforts have usually been limited to predicting the peak locations of spectral structure, not the relative strengths of different peaks nor the shape of a whole spectrum. One aim of this paper is to demonstrate that such further calculations are straightforward, at least in the context of the models that have been so successful in fitting peak locations. Comparisons of such calculations with experimental data should be helpful in refining the understanding of surface electronic structure. A second goal is to exhibit how spectra change when surface states become surface resonances, due to the phase-matching energy moving out of a forbidden gap and/or above the vacuum level. For such cases the peak locations predicted by the multiple-reflection picture are not generally reliable and matrix element effects become important. We showed in an earlier paper¹⁰ that in the extreme limit of a jellium model the spectral structure near the vacuum threshold is better interpreted as due to interference maxima and minima rather than as a set of surface resonances. Here we exhibit how this picture evolves into one of surface resonances and then true surface states as an electron's ability to penetrate the barriers decreases.

In the next section we briefly present the equations that

define our model of inverse photoemission and note their relation to previous work. Then in Sec. III we describe calculations that illustrate the range of possible behavior. Although we do not attempt to fit spectral data, we point out that some qualitative features of our results that have been observed.

II. MODEL

The basic idea is to use the one-electron eigenstates implicit in the simplest multiple-reflection picture to calculate inverse-photoemission spectra. Begin with the effective potential energy. We use the one-dimensional form employed in the systematic study of Ref. 8; see Fig. 1. Taking x as the coordinate along the surface normal, with the metal in the region $x > 0$, we write

$$V(x) = \begin{cases} V_C(x), & 0 < x \\ V_B(x), & x < 0, \end{cases} \quad (1)$$

where the crystal potential is described by a single (pseudo)potential coefficient V_g ,

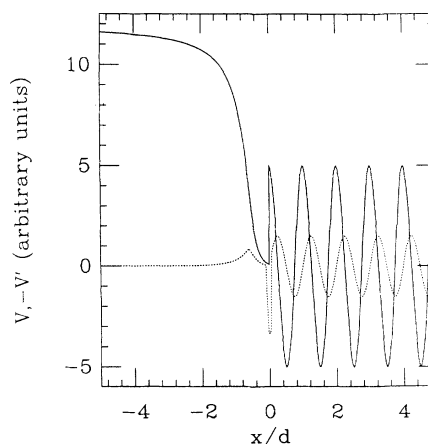


FIG. 1. The electron potential energy and its gradient vs position along the surface normal. The solid curve is V ; the dashed curve is $-V'$. The pseudopotential parameters $V_g = 2.5$ eV here and the last layer of atoms is at $x = 0$. The other parameters are given in the text. Note how quickly the coupling function V' decays as one moves into vacuum.

$$V_C(x) = 2V_g \cos(gx). \quad (2)$$

We are considering only the simple case (relevant to {100} or {111} surfaces) where the reciprocal-lattice vector responsible for the Bragg scattering of interest also lies along the surface normal. Its length, $g = 2\pi/d$, is determined by the spacing d between layers of atoms. Eigensolutions in the crystal are Bloch waves, which we find in a two-plane-wave approximation as a linear combination of e^{ikx} and $e^{i(k-g)x}$. The Bloch wave vector k is real valued in the allowed bands and complex valued in the forbidden energy gap.

For the surface barrier we write¹¹

$$V_B(x) - U_0 = \begin{cases} -\frac{e^2/4}{|x-x_0|} (1 - e^{-\lambda|x-x_0|}), & x < x_0 \\ -U_0/(1 + Ae^{-\beta|x-x_0|}), & x_0 < x. \end{cases} \quad (3)$$

The parameters A and β are fixed by requiring V_B to be continuous in value and slope at $x = x_0$. This leaves U_0 , λ , and x_0 to be chosen. Solutions of Schrödinger's equation with V_B are found by numerical integration.

Eigenfunctions of the total potential energy V are obtained by matching half-space solutions across the plane at $x = 0$. These may carry a net current either into or out of the crystal or possibly no current at all. The latter case has several subcases, depending on whether the eigenvalue lies in the forbidden gap or below the vacuum threshold or both. It is only for the last subcase that one has a true surface state.

The calculation of inverse photoemission is easy to formulate if one exploits its close relation to photoemission.^{12,13} Our procedure here is similar to what we did in the jellium-model calculations.¹⁰ The eigenvalue spectrum is now more complicated, having both continuous ranges within bands and discrete values within a gap, and one must take care to use a proper normalization scheme.¹⁴ However, the present calculations are also less sophisticated than the earlier ones in that we completely ignore the spatial variation of the photon field. Such an approximation in jellium can change the predicted yield by orders of magnitude,¹⁰ but does not strongly distort its qualitative shape. It has the numerical advantage that one only needs matrix elements of the gradient of the potential energy. For the V of Eq. (1), there is a discontinuity at $x = 0$ which leads to a δ -function term in $V' = dV/dx$. In Fig. 1 (but not in the calculations of Sec. III) we spread out this spike over a distance $0.07d$ to make its relative strength apparent. In more realistic treatments such spikes would be absent if V were everywhere continuous.

The quantity we have calculated is proportional to a differential yield and is defined by the Fermi-golden-rule combination of one-dimensional matrix elements

$$Y \propto \frac{1}{2\pi} \sum_f \left| \left\langle \psi_i \left| \frac{dV}{dx} \right| \psi_f \right\rangle \right|^2 \left| \frac{dq}{dE_f} \right| + \sum_s \left| \left\langle \psi_i \left| \frac{dV}{dx} \right| \psi_s \right\rangle \right|^2 \delta(E_s + \hbar\omega - E_i), \quad (4)$$

where ψ_i and E_i refer to the initial state and $\hbar\omega$ is the photon energy. The final states have a subscript f if they lie in a continuum and a subscript s if they are discrete (i.e., true surface states). The $|\psi_s\rangle$ are normalized so that

$$\langle \psi_s | \psi_{s'} \rangle = \delta_{s,s'}, \quad (5)$$

while for the continuum states with a common form

$$\langle \psi_f | \psi_{f'} \rangle = 2\pi\delta(q - q'), \quad (6)$$

where the wave vector q here and in Eq. (4) may be either a Bloch wave vector or an asymptotic free-electron wave vector in vacuum, depending on the form of the final state.¹⁴

In order to compare the relative strength of the two contributions in Eq. (4) we will convolve the E_f dependence of the raw spectrum with a Gaussian. This is the only broadening that we introduce. If there are transitions that conserve crystal momentum, the above procedure is inadequate where they contribute. Rather than generalize our method for these cases, we simply do not examine such regions of E_f space. Our rationale is twofold: First, our present interest lies in the surface, not bulk, transitions, and second, the existing formalisms for treating surface and bulk transitions on a common basis are computationally intensive,^{12,15} and hence, although more realistic, are neither as flexible nor as transparent as our scheme.

There remains the choice of parameter values. We fix the photon energy at 9.7 eV and take the potential parameters as mostly those of the (111) face of Cu.⁸ Thus $d = a/\sqrt{3}$ with $a = 3.61$ Å, $x_0 = -1.27$ Å, $\lambda = 0.62$ Å, and $U_0 = 11.99$ eV, which follows from a work function of 4.94 eV and a free-electron Fermi energy of 7.05 eV. The remaining parameter is V_g , which for the L gap in Cu should be about 2.5 eV; but we shall calculate for a range of values of V_g . Thus in effect we hold the surface-state or resonance positions (nearly) fixed and vary the band-edge locations. We note that a similar calculational approach has been used by Jurczyszyn,¹⁶ but he examined only the density of final states, not the matrix elements found here. By comparing his figures with ours, it is obvious that the influence of the matrix elements on the shape of the spectra is significant. Still the Green's-function approach he uses,^{16,17} or the alternate one developed by Radny,¹⁸⁻²⁰ may provide a convenient way to treat the direct transitions we avoid.

III. CALCULATIONS

A collection of our results is presented in Figs. 2 and 3, which show the behavior of Y near the upper and lower band edges, respectively. In the spirit of a qualitative survey we have ignored the constraints of the Fermi level, which for Cu is near 7 eV. However, we have not shown calculations below $E_f = 6$ eV because the direct (momentum-conserving, bulk) transition around $E_f \approx 4$ eV rapidly becomes dominant. The broadening parameter for all cases is 0.2 eV full width at half maximum, which generally blurs out all but the first image-potential state or resonance.

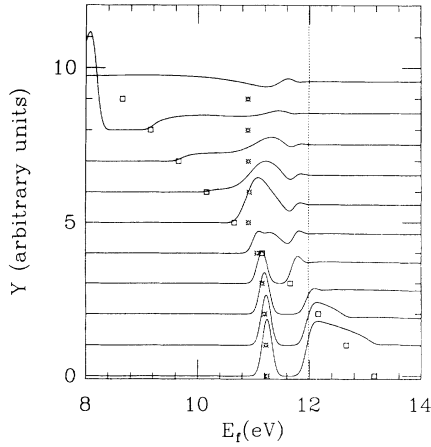


FIG. 2. Inverse-photoemission yield Y vs final-state energy E_f . The electrons are incident along the surface normal and the photon angular dependence has been factored away (see Ref. 10). The different curves are for different values of V_g , which runs from 0 to 4.5 eV in steps of 0.5 eV as one moves from the top to the bottom of the picture. The origin for Y jumps by one unit between curves. Along each $Y=0$ level the squares denote the upper edge of the band gap and the bursts give the surface-state or -resonance prediction of the phase-accumulation model. The vertical dashed line marks the vacuum level.

As V_g increases, one leaves the jellium limit by developing band edge and surface resonances, and the latter eventually becomes true surface states. In both figures we have indicated where the multiple reflection argument would predict the surface states and/or resonances to be. The location of each burst symbol is determined by minimizing $|1-r_B r_C|$, where r_B and r_C are the complex-

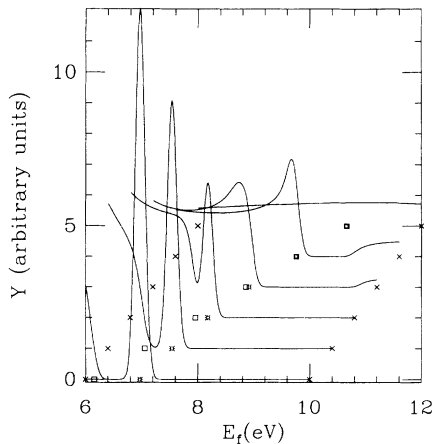


FIG. 3. Inverse-photoemission yield Y vs final-state energy E_f . The plotting scheme is essentially the same as Fig. 2 except that the curves have been shifted both vertically and horizontally for clarity. The squares now locate the lower edge of the band gap and the bursts again are the predicted location of surface states and/or resonances. The pair of crosses along each $Y=0$ level marks the range of E_f between 6 and 10 eV. From top to bottom the value of V_g ranges from 0 to 2.5 eV in steps of 0.5 eV.

valued reflection amplitudes from V_B and V_C , respectively. When the energy lies below the vacuum threshold $|r_B|=1$, while when it is inside the band gap $|r_C|=1$. When both constraints are satisfied, we can write $r_B=e^{i\phi_B}$ and $r_C=e^{i\phi_C}$, with real-valued ϕ_B and ϕ_C . Then the minimum of $|1-r_B r_C|$ becomes the well known requirement¹⁻⁵

$$\phi_B + \phi_C = 2\pi n \quad (7)$$

with n an integer. The solutions of Eq. (7) give the exact surface-state locations, but when either r does not have unit magnitude, Eq. (7) is not relevant and even the location of a minimum in $|1-r_B r_C|$ is only suggestive of where the peak in Y will occur, not a rigorous prediction. This is especially evident in Fig. 2, where the first image-potential-state peak broadens and shifts away from its predicted location as it moves into the upper band.

In Fig. 4 we plot a summary of energy locations of structure in our results. For true surface states the predicted and "observed" locations agree perfectly, but for surface resonances there is in general no agreement. We have also shown in Fig. 4 the location of other peaks in Y which are not related to surface states and/or resonances. They arise from a variety of causes. Those just inside a band we call band edge effects and discuss in more detail below. Those above the vacuum level are due to a peak in the distribution of the inverse of band-gap photoemission.²¹ As is evident from the bottom three curves in Fig. 2, these peaks are the maxima of quite broad structures and would be difficult to identify experimentally. We only stress that in our calculation these peaks are not due to higher members of the image-potential-state series, which always lie below the vacuum level and are in addition quite weak. For instance, when

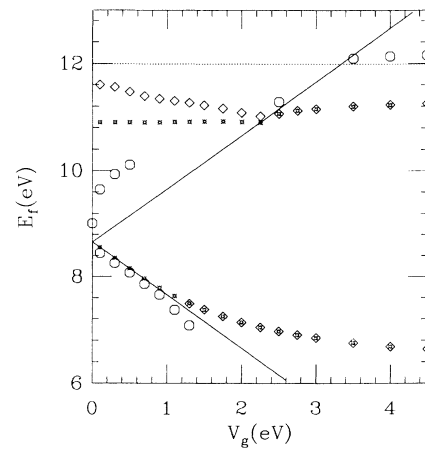


FIG. 4. Final-state-energy locations of peaks in the inverse-photoemission yield vs the strength of the pseudopotential. These locations are extracted from curves such as in Figs. 2 and 3. For reference the solid lines give the band-gap positions and the dashed line is the vacuum level. The diamonds are peak locations associated with surface states and/or resonances; the octagons describe peaks produced by other causes (see text); and the bursts are where the multiple-reflection model predicts peaks should be.

$V_g = 4.5$ eV, the (visible) first image-potential-state contribution to Y at 11.24 eV is seven times stronger than that of the (invisible) next image-potential state at 11.78 eV. This weakening of the excitation efficiency is easy to rationalize because the higher image-potential states sit farther out in vacuum where the coupling V' in Fig. 1 is smaller. The other additional peaks between 9 and 10 eV at small V_g are also associated with very broad structures and arise from gradual changes in both the matrix elements and the density of states.

Returning to Figs. 2 and 3 we now discuss in more detail the cause and evolution of structures. The strength of Y is generally greater for final states near the top of the lower band than for states near the bottom of the higher band. This difference is due to different symmetries of the eigenstates and persists even as $V_g \rightarrow 0$, as we illustrate in Fig. 5. For the range of V_g used in this figure no surface states yet exist. The increasingly strong peak just below the lower band edge might be interpreted either as a surface resonance or as a bulk band-edge effect. The two locations stay close over an extended range of V_g as shown in Fig. 4. This surface resonance becomes the Shockley surface state for $V_g \geq 0.5$ eV but it remains too weak and too close to the band edge to be seen separately until V_g reaches 1.3 eV. Near the same values of V_g the band-edge peak is moving away from the edge and becoming merely a shoulder on the incipient direct transition. Returning to Fig. 5 we note that in spite of the strong changes near the band edges, the values of Y just below the vacuum threshold are hardly affected, so the peak that appears near 11.6 eV is essentially due to interference effects in the matrix elements.¹⁰

This peak does eventually change as V_g increases, shifting down and nearly disappearing when V_g reaches 0.5 eV, then sharpening and continuing to shift towards the predicted resonance location as the growing V_g puts it closer to the band edge. This surface resonance becomes especially strong just before it enters the band gap as the

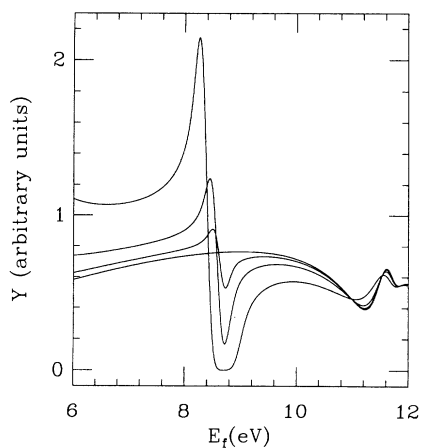


FIG. 5. Inverse-photoemission yield Y vs final-state energy E_f . The configuration is the same as in Figs. 2 and 3 and V_g equals 0.0, 0.03, 0.1, or 0.3 eV. Note the contrasting behavior at the two band edges and the minimal changes near the vacuum level.

first image-potential state. In Fig. 6 we show in more detail how the surface resonance transforms into a surface-state peak. The surface state already exists at $V_g = 2.4$ eV but its excitation strength is too weak to produce structure discernible from that due to the band edge. At $V_g = 2.6$ eV, one has two peaks below 11.5 eV. The low-energy one is due to the first image-potential state while the second one is a band-edge peak, lying just above the band edge at 11.26 eV. The higher image resonances are clumped into the peak just below the vacuum level.

After a surface resonance has become a surface state (with initially zero excitation strength), it quickly, but continuously, grows in excitation strength as its energy moves away from the band edge. This holds for both the Shockley and image-potential states. One might think that the order-of-magnitude difference in excitation strength between the two could be understood by the same reasoning as used earlier for the successive image-potential states. However, we find that interference effects in the matrix elements are important, especially for the Shockley state whose eigenfunction overlaps strongly with both the bulk and surface parts of V' .

Since it is unreasonable to claim *a priori* that our model calculations should reproduce real data, we take an empirical approach and simply note two areas of qualitative agreement. For Cu(111),²² the relative excitation strength of the two surface states agrees with our calculations. For Au(111),²³ the image resonance is more than an eV inside the upper band, which roughly corresponds to our case of $V_g = 1.5$ eV, and is shifted above the location predicted by the phase-accumulation model by several tenths of an eV. The sign and magnitude of this shift is consistent with our results in Figs. 2 and 4. These favorable comparisons suggest that further cases should be considered, adjusting the form of V to give not only peak positions but also strengths and widths. It would also be interesting if the detailed behavior shown in Fig. 6 could be confirmed. The standard way in which one ob-

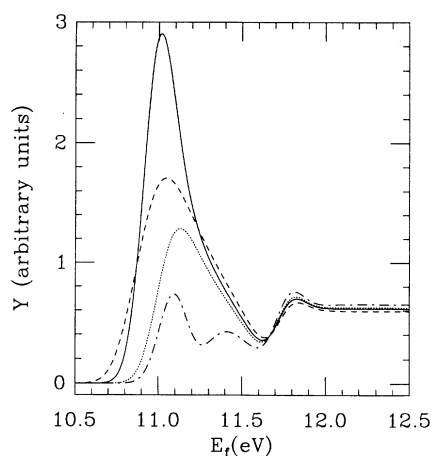


FIG. 6. Inverse-photoemission yield Y vs final-state energy E_f . The configuration is the same as in Figs. 2 and 3 and $V_g = 2.1$ eV (long-dashed line), 2.3 eV (solid line), 2.4 eV (short-dashed line) and 2.6 eV for (dash-dotted line).

serves a surface state transforming into a surface resonance is by varying the parallel momentum.^{24,25} For our simple model this would not happen since formally the band edge and any surface state or resonance would shift at the same rate. One needs to mix in more plane waves in the theory to produce a relative motion of a band edge and a surface state or resonance with parallel momentum. Such a theoretical effort would probably require more complete theories^{12,15} to produce reliable results.

ACKNOWLEDGMENTS

We thank Yong Wang and Dr. Neville Smith for helpful discussions. Our work was supported in part by the National Science Foundation through Grant No. DMR-89-03851. Some of the calculations were done on the Cray Research, Inc. Y-MP4/464 system at the National Center for Supercomputing Applications at the University of Illinois at Urbana-Champaign (Champaign, IL).

¹N. V. Smith, Rep. Prog. Phys. **51**, 1227 (1988).

²P. M. Echenique and J. B. Pendry, Prog. Surf. Sci. **32**, 111 (1989).

³P. M. Echenique and J. B. Pendry, J. Phys. C **11**, 2065 (1978).

⁴E. G. McRae, Rev. Mod. Phys. **51**, 541 (1979).

⁵N. V. Smith, Phys. Rev. B **32**, 3549 (1985).

⁶C. T. Chen and N. V. Smith, Phys. Rev. B **35**, 5407 (1987).

⁷M. Ortuno and P. M. Echenique, Phys. Rev. B **34**, 5199 (1986).

⁸N. V. Smith, C. T. Chen, and M. Weinert, Phys. Rev. B **40**, 7565 (1989).

⁹N. V. Smith and C. T. Chen, Surf. Sci. **247**, 133 (1991).

¹⁰W. L. Schaich and J.-T. Lee, Phys. Rev. B **44**, 5973 (1991).

¹¹R. O. Jones, P. J. Jennings, and O. Jepsen, Phys. Rev. B **29**, 6474 (1984).

¹²J. B. Pendry, J. Phys. C **14**, 1381 (1981).

¹³P. D. Johnson and J. W. Davenport, Phys. Rev. B **31**, 7521 (1985).

¹⁴W. L. Schaich, in *Photoemission in Solids*, edited by M. Cardona and L. Ley (Springer, New York, 1978), Vol. 1.

¹⁵G. Borstel and G. Thörner, Surf. Sci. Rep. **8**, 1 (1987).

¹⁶L. Jurczyszyn, Surf. Sci. **247**, 158 (1991).

¹⁷M. Radny, Surf. Sci. **231**, 43 (1990).

¹⁸M. Radny, J. Phys. **CM2**, 4661 (1991).

¹⁹M. Radny, Surf. Sci. **247**, 143 (1991).

²⁰M. Radny, J. Phys. **CM3**, 5525 (1991).

²¹D. A. Wesner, P. D. Johnson, and N. V. Smith, Phys. Rev. B **30**, 503 (1984).

²²S. L. Hulbert *et al.*, Phys. Rev. B **31**, 6815 (1985).

²³D. P. Woodruff, W. A. Royer, and N. V. Smith, Phys. Rev. B **34**, 764 (1986).

²⁴E. Kneedler, D. Skelten, K. E. Smith, and S. D. Kevan, Phys. Rev. Lett. **64**, 3151 (1990).

²⁵S. Yang, K. Garrison, and R. A. Bartynski, Phys. Rev. B **43**, 2025 (1991).